

SDS Micelles at High Ionic Strength. A Light Scattering, Neutron Scattering, Fluorescence Quenching, and CryoTEM Investigation

M. Almgren,^{*1} J. C. Gimel,^{*2} Ke Wang,^{*} G. Karlsson,^{*} K. Edwards,^{*} W. Brown,^{*} and K. Mortensen[†]

^{*}Department of Physical Chemistry, Box 532, University of Uppsala, S-751 21 Uppsala, Sweden; and

[†]Department of Solid State Physics, Risø National Laboratory, DK-4000 Roskilde, Denmark

Received March 21, 1996; accepted March 5, 1998

Sodium dodecyl sulfate (SDS) in 0.8 M NaCl in D₂O has been studied by small-angle neutron scattering (SANS), dynamic light scattering (DLS), and time-resolved fluorescence quenching (TRFQ) measurements in the concentration range from 10 to 80 mM and at temperatures from 25 to 45°C. Examination by cryo-transmission electron microscopy revealed the presence of a variety of structures, from broad band-like or lace-like aggregates to multiconnected threads. It is suggested that these structures are formed at the air–solution interface. To verify that they are not present in the bulk solution, SANS, DLS, and TRFQ were studied on the same solutions. The SANS results confirm, on the length scale available using this technique, a local cylindrical structure for the micelles. Assuming a rod model, with the slow mode corresponding to translational diffusion and the fast mode to the rotational dynamics of cylindrical SDS micelles, the DLS data at 25°C in 0.8 M NaCl would correspond to a hydrodynamic length $L \approx 150$ nm, employing a radius of about 2 nm. The TRFQ shows a transition from small micelles at high temperature and low surfactant concentration to long structures at low temperature and high concentration. © 1998 Academic Press

Key Words: surfactant; micelles; SANS; dynamic light scattering; fluorescence quenching; cryoTEM; sphere-to-rod transition; interfacial aggregates.

INTRODUCTION

In common with many other ionic surfactants, sodium dodecyl sulfate (SDS) forms rod-like micelles at high concentration and high ionic strength. This was demonstrated in the pioneering X-ray studies by Reiss-Husson and Luzzati (1). In an attempt to visualize such micelles, SDS in 0.8 M NaCl was investigated by cryo-TEM. In this method a very thin film of the aqueous solution is rapidly vitrified, and directly examined at liquid nitrogen temperature in a transmission electron microscope (2, 3). Dynamic and solvent-dependent structures can be captured and examined, and

both rods and thread-like micelles have been observed in various surfactant systems (3). In the investigation of the SDS micelles, however, rather strange and unusual structures were found, as described below. The micrographs have features suggesting that the observed aggregates were present at the air–liquid interfaces but not in the bulk solution. This is important and is regarded either as an artefact of the cryo-TEM method or as a new possibility for the study of aggregates at interfaces. To ensure that the structures were not already present in the solution, we decided to study the aggregation using several methods on the same solution as used in the cryoTEM study.

SDS micelles in aqueous salt solutions have been investigated with various methods in numerous studies following the work of Reiss-Husson and Luzzati. A critical account of investigations using small angle scattering methods was given by Cabane (4) and of static and dynamic light scattering by Candau (5), Magid (6), and Schurtenberger (7).

Mazer and co-workers (8–10) made extensive light scattering measurements on SDS and related surfactants and interpreted the results using a simple thermodynamic “ladder” model for the growth of rod-like micelles. In essence, the model assumes the surfactant to be present in two distinct states in the micelles, either in the cylindrical portion or in the half-spherical endcaps. Such a model implies, as has been shown earlier by others (11, 12), that the rod-like micelles have a broad, exponential size distribution starting from the minimum size of a spherical micelle without a cylindrical region. The weight average aggregation number, at given salt concentration, should be proportional to the square root of the surfactant concentration. The results could be given a consistent interpretation within the model, and even if the investigation can be questioned in many details—for instance, intermicellar interactions are not considered—the picture that emerges probably captures the essential features of the systems.

Corti and Degiorgio (13) used the same methods in their study of the same system and addressed in particular the intermicellar interactions, as modeled with the DLVO theory. Their analysis of the results, for salt concentrations

¹ To whom correspondence should be addressed.

² Present address: Laboratoire de Physico-Chimie Macromoléculaire, Université du Maine, Route de Laval, 72017 Le Mans Cedex, France.

up to 0.6 M NaCl, indicated only a slight increase of the aggregation number (in this analysis obtained by extrapolation to zero surfactant concentration). A strong increase in size with surfactant concentration at high ionic strength was not ruled out; the authors speculated about the formation of linear clusters of globular micelles as a result of attractive interactions. It is not clear, however, if both interactions and aggregation numbers can be determined from the concentration dependence of the scattering, when a growth of the micelles occurs. To our knowledge, no completely satisfactory analysis has been presented. In a more recent study, Mishic and Fisch (14) combined dynamic and static light scattering in an attempt to determine the flexibility of the rods in SDS solutions at high salt concentration (0.8 and 1.0 M NaCl).

In further light scattering contributions, Hayashi and Ikeda (15) and Ikeda *et al.* (16) confirmed the growth of the micelles at high salt concentrations and also discussed the flexibility of the rods. The authors noted an anomalous angle dependence of the scattered intensity under certain conditions and speculated about the formation of clusters of micelles ("microgels") as a possible reason for the interaction. The anomalous angle dependence, which was not accompanied by an increased scattering at 90°, occurred at high salt concentration and at a temperature just above the Krafft point.

Cabane (4, 17) presented a high-resolution SANS study, from which it is clear that long rod-like micelles are present at high salt concentration (rather than clusters of spheres). He also observed, for SDS in 0.8 M NaBr at 25°C, that the intensity at very low values of the scattering vector, increased above that for the cylinder model, and proposed that microcrystals of the surfactant could be responsible for this peak.

Even if the earlier results show convincingly that rod-like micelles (although probably flexible) are the prevalent structures at high salt concentration and low temperature, the available results are not clear about the intermicellar interactions; could the observed cryo-TEM structures arise from a clustering of rod-like micelles in the bulk solution? To resolve this question, a set of samples was investigated with cryo-TEM and dynamic light scattering, as well as with SANS (the latter method dictated the choice of D₂O as solvent), to give directly comparable results. The measurements were complemented with time-resolved fluorescence quenching studies, from which average aggregation numbers are obtained when the micelles are small and which would indicate a transition to long micelles by a clear, qualitative change in the decay curves (18, 19).

EXPERIMENTAL AND DATA ANALYSIS

Sample Preparation

Sodium dodecyl sulfate, especially pure grade (from BDH), was used without further purification. SDS solutions

in 0.8 M NaCl were prepared in D₂O for neutron scattering experiments. The solutions were prepared and stored at 45°C. When stored at room temperature precipitation occurred, in line with the fact that the critical micellar temperature has been reported to be close to (16) or even above (20) 25°C in 0.8 M NaCl solution. The samples were analysed at three different temperatures, 45, 35, and 25°C, in this order, and no visible turbidity was apparent during the measurements at the lowest temperature. It is possible that the SDS preparation was not completely pure, which would lower the critical temperature; otherwise the measurements at 25°C were performed on undercooled samples. This is not expected to be a problem. Crystallization below the critical temperature does not occur by aggregation of micelles and would not be accompanied by attractive interactions between the micelles that could interfere with the scattering measurements or produce a secondary aggregation that could explain the cryo-TEM micrographs.

Prior to the dynamic light scattering measurements, the warm samples were filtered through 0.1 μm pore size Anotop filters into glass ampules that had been soaked in chromic acid and rinsed with distilled water and filtered ethanol. The use of a filter pore size close to or even smaller than the characteristic size of the structures is not a risk for changing the concentration with dynamic micelles; any disruption occurring during the passage of a narrow pore would be reversible and not expected to influence the equilibrium size distribution. For SANS measurements, the samples were mounted in sealed quartz containers (Suprasil from Hellma, FRG), with 2 mm flight path. The neutron spectrum of water, used for calibration, was obtained in a 1 mm thick quartz cuvette.

Dynamic Light Scattering

Dynamic light scattering measurements were performed using a Coherent Innova Ar ion laser operating at 488 nm. The scattering cells were immersed in a large diameter thermostated bath of decalin. Both the incident beam and the scattered light were vertically polarized using a Glan-Thompson polarizer (extinction 10⁻⁶). The detector optics included a 4 μm diameter monomodal fiber coupled to an ITT FW130 photomultiplier. The output was digitized by an ALV-PM-PD amplifier-discriminator, and the signal was analyzed with an ALV-5000 digital multiple τ correlator with 288 exponentially spaced channels. It has a minimum sampling time of 0.2 μs and a maximum of about 100 s. Measurements were performed at different scattering angles, θ, giving a q range of (5.9–25) × 10⁻⁶ Å⁻¹, where q = (4πn_s/λ₀) sin(θ/2), with n_s the refractive index of the solution (1.33 for aqueous solutions) and λ₀ the wavelength of the radiation in vacuum.

The DLS measurements were performed in the homodyne mode (21). The data were analyzed by a nonlinear regression procedure. g₂(t) is the measured normalized intensity

autocorrelation function. It is related to the normalized field autocorrelation function, $g_1(t)$, through the Siegert relation:

$$g_2(t) - 1 = \beta |g_1(t)|^2, \quad [1]$$

where β is a nonideality factor ($0 < \beta \leq 1$). $g_1(t)$ can be written as the Laplace transform of the distribution of relaxation rates, $G(\Gamma)$:

$$g_1(t) = \int_0^\infty G(\Gamma) \exp(-\Gamma t) d\Gamma, \quad [2]$$

where Γ is the relaxation rate. In terms of the corresponding relaxation times, τ , $g_1(t)$ will be expressed here as

$$g_1(t) = \int_{-\infty}^\infty \tau A(\tau) \exp(-t/\tau) d \ln \tau, \quad [3]$$

where $\tau A(\tau) \equiv \Gamma G(\Gamma)$ on a logarithmic scale. $\tau A(\tau)$ was obtained by regularized inverse Laplace transform (RILT) of the experimental data using a constrained regularization calculation algorithm called REPES (22–24) which is essentially similar to CONTIN (25), except that REPES directly minimizes the sum of the squared differences between experimental and calculated $g_2(t)$ functions. For a diffusion process in the limit of small q , the average relaxation rate of a particular mode, $\langle \Gamma \rangle$, is q^2 dependent and is related to the translational mutual diffusion coefficient D_m as

$$\langle \Gamma \rangle = D_m q^2. \quad [4]$$

Small-Angle Neutron Scattering

The measurements were carried out at the Risø SANS facility. Scattering data were obtained using neutrons with wavelength $\lambda = 1.50$ or 0.65 nm. The sample-to-detector distance was 3 m, giving a q range of $(4 \times 10^{-5}) - (4 \times 10^{-4}) \text{ \AA}^{-1}$ and $10^{-4} - 10^{-3} \text{ \AA}^{-1}$, respectively. The neutron wavelength resolution was $\Delta\lambda/\lambda = 0.18$, and the beam divergence was determined by a collimation length of 3 m with pinhole sizes 16 and 7 mm in diameter at the source and sample positions, respectively. The scattering data were corrected for background arising from the quartz container with D_2O and from other sources, as measured with the neutron beam blocked by plastic containing boron at the sample position. The incoherent scattering from H_2O was used to take into account deviation from uniform detector response and to bring the data to an absolute scale, according to standard procedure (26).

The neutron scattering data were all azimuthally isotropic. The data have therefore been reduced to the one-dimensional $I(q)$ scattering functions which are only dependent on the absolute value of q . From Bendedouch *et al.* (27) and Sheu

et al. (28) it appears that for SDS micelles in D_2O the scattering length density of the outer hydrophilic region of hydrated polar head groups closely matches the scattering length density of the solvent, $\rho_{D_2O} = 6.34 \times 10^{-11} \text{ cm}^3/\text{nm}^3$. Therefore, the scattering function is determined by the inner hydrophobic core of compact hydrocarbon chains. The SANS scattering results were fitted to various analytical model functions. Least-squares fitting, including instrumental smearing, showed that the data agreed best by a model for rod-like micelles with the expression (29)

$$I(q) = c \Delta\rho_m^2 \int_0^{\pi/2} \frac{2B_1(qR \sin \alpha)}{qR \sin \alpha} \times \frac{\sin(qL \cos \alpha)/2}{qL \cos \alpha/2} \sin \alpha d\alpha, \quad [5]$$

where $q = (4\pi/\lambda) \sin(\theta/2)$ is the scattering vector, λ is the neutron wavelength, θ the scattering angle, and α is the angle between rod-director and scattering vector. R and L are the radius and the length of the rod-like micelle, respectively, and B_1 is the first-order Bessel function. c is the concentration, and $\Delta\rho$ is the scattering contrast factor. More elaborate models including micelle flexibility and length polydispersity would fit the data equally well, but the inclusion of further parameters was not warranted for the available data.

Time-Resolved Fluorescence Quenching (TRFQ) Data

The single-photon counting set up has been described in detail earlier (30). Pyrene at a low concentration was employed as the hydrophobic probe and dimethylbenzophenone as quencher, at concentrations corresponding to less than one quencher per micelle for small micelles. To increase the accessible time window, the samples were deaerated by freeze–pump–thaw cycles.

TRFQ data treatment. Rapid quenching occurs in small micelles containing quenchers. Excited states survive to long times only in micelles without quenchers, and decay with the same decay constant, k_0 , as in a solution without quenchers. A characteristic decay pattern is the result, with parallel tails in a semilogarithmic plot, that can be analyzed using the simplified Infelta–Tachiya model (19, 31, 32) to obtain the aggregation numbers:

$$\ln[F(t)/F(0)] = -k_0 t + \langle n \rangle \{ \exp(-k_q t) - 1 \}. \quad [6]$$

$F(t)$ and $F(0)$ are the fluorescence intensities at time t and at the moment of excitation, respectively, $\langle n \rangle = [Q]_m / [\text{mic}]$ is the average number of quenchers per micelle, and k_q the first order rate constant for quenching in a micelle with one quencher. With the concentration of micellised surfactant known, an average aggregation number is obtained from $\langle n \rangle$, as discussed earlier (19). Most of the sam-

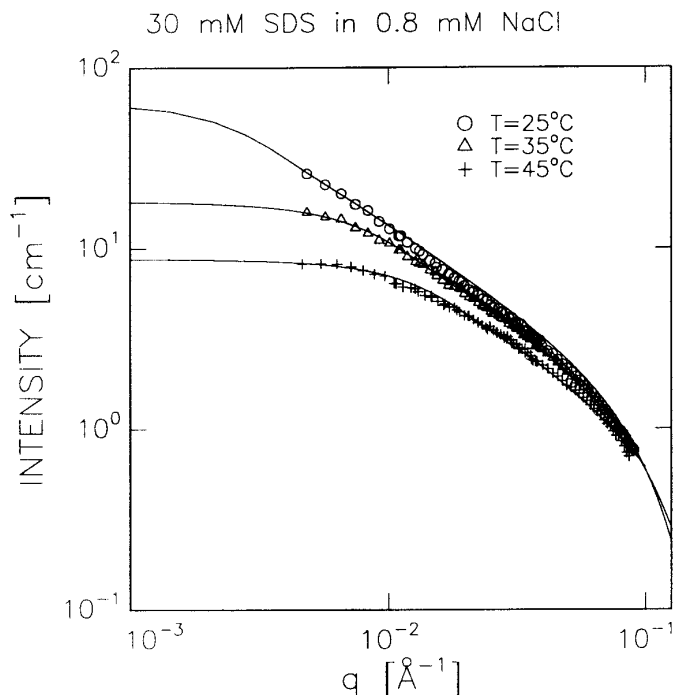


FIG. 1. Neutron scattered intensity $I(q)$, as a function of the scattering vector, q , for a solution of 30 mM SDS in 0.8 M NaCl at different temperatures: (+) 45°C, (Δ) 35°C, and (\circ) 25°C.

ples in this study contained micelles which were too long for the model to apply and reliable aggregation numbers could be obtained only from the results at the lowest SDS concentration and the highest temperature.

The model and procedure for diffusion-controlled quenching in one-dimensional cylinders were discussed in Refs. (19, 33, 34). In infinitely long micelles, i.e. for $L \gg D\Delta t$, where Δt is the time window of the measurement and D the sum of the diffusion coefficients of the excited probe and quencher in the micelle; all excited probes are accessible for quenching, and the decay curves do not attain a final exponential tail. An analysis of the data can only give the product DR^4 (34), where R is the radius of the cylinder in which the reactants are confined. This model applies at high SDS concentrations and low temperature.

Cryo-TEM. Within a chamber of controlled humidity and temperature, a small drop of the sample was deposited on a copper grid covered by a porous polymer film. After careful spreading of the drop, excess liquid was blotted away with filter paper. By this technique, thin (100–500 nm) sample films, spanning the $\sim 5 \mu\text{m}$ large holes in the polymer film, were formed. After blotting, the sample was plunged into liquid ethane kept just above the freezing temperature. The vitrified sample was transferred under liquid nitrogen to a Zeiss EM 902 electron microscope. During examination the specimen temperature was kept below 108 K, and all observations were made in zero-loss brightfield mode at an accelerating voltage of 80 kV.

RESULTS AND DISCUSSION

Figures 1 and 2 show the influence of temperature and concentration on the neutron scattered intensity. The best fits to the cylinder model of Eq. [5] are shown as solid lines. As mentioned above, the scattering length density of the D_2O and the hydrated head groups match closely, whereas there is significant contrast with the hydrocarbon micellar core. Fits to the cylinder model, independent of SDS concentration and temperature, gave a micellar core radius of the order of $1.9 \pm 0.1 \text{ nm}$.

The micelle length varies with temperature and concentration. The sample with 30 mM SDS in 0.8 M NaCl contains rod-like micelles which at 25°C have a length of the order of $L = 160 \text{ nm}$. At 35°C, $L = 47 \pm 1 \text{ nm}$, and at 45°C, $L = 31 \pm 1 \text{ nm}$. At a fixed temperature of 45°C, the average micelle length varied as 15, 29, 31, and $33 \pm 1 \text{ nm}$ for concentrations of 10, 30, 50, and 80 mM, respectively. Since the flexibility and polydispersity were not taken into account in the model, the length estimates are very uncertain, even as averages or persistence lengths.

In Fig. 3 is shown the forward scattering, $I(0)$, normalized by the SDS concentration, plotted versus resulting micellar rod length. We see a nearly perfect linear relationship between $I(0)$, which represents the micellar mass, and the micellar rod length, as if the SDS micelles really were rod-like, and not worm-like aggregates where the length ob-

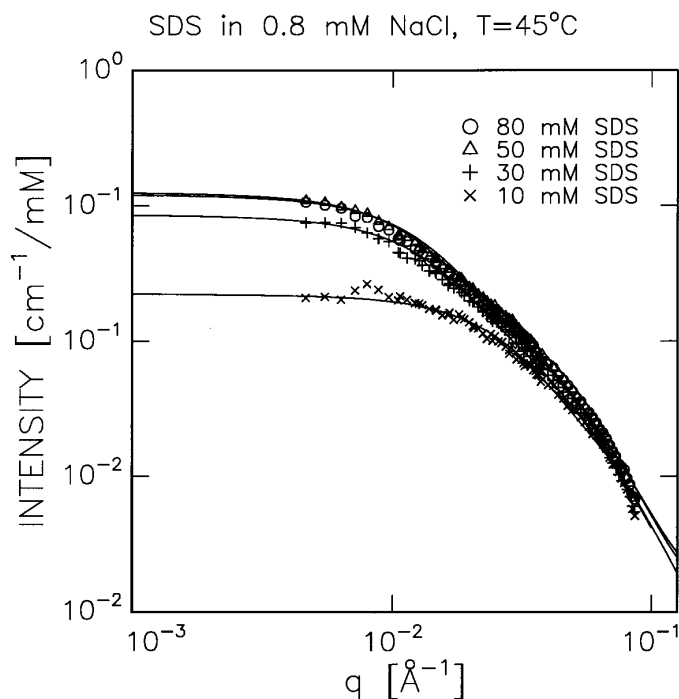


FIG. 2. Neutron scattered intensity normalized by concentration, $I(q)/c$, as a function of the scattering vector, q , at 45°C for SDS solutions in 0.8 M NaCl at various concentrations: (\times) 10 mM, (+) 30 mM, (Δ) 50 mM, and (\circ) 80 mM.

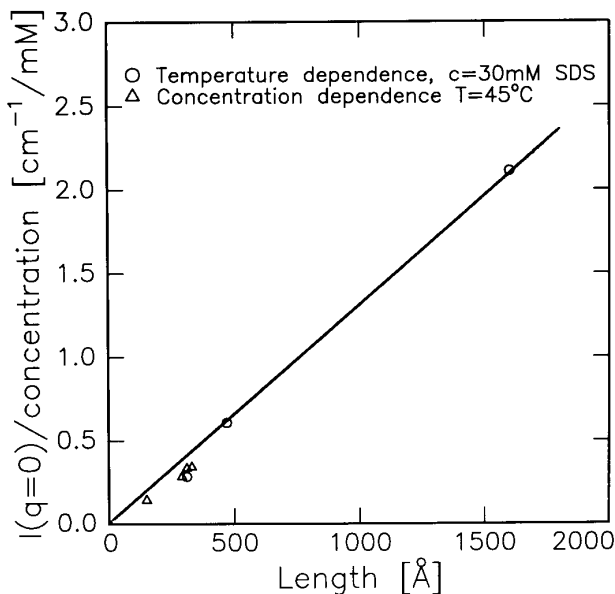


FIG. 3. Forward scattering from SANS, normalized by concentration, plotted against the estimated rod length.

served from SANS would be interpreted as a persistence length.

The $I(0)$ versus micellar length can be used to gain information on the micellar mass per unit length. The total micellar mass is given by

$$M = \frac{I(0)}{c} \frac{10^3}{N_A \Delta \rho_m^2}, \quad [7]$$

where c is the concentration in mg/mL (the factor 10^3 converts mg to g), N_A is Avogadro's number, b the scattering length, and $\Delta \rho_m$ is the scattering contrast per unit mass:

$$\Delta \rho_m = M_{CH}^{-1} (\Sigma_{CH} b - \rho_{D_2O} V_{CH}), \quad [8]$$

where the index CH denotes that the molecular mass and the sum over scattering lengths, b , refers to the hydrocarbon part of the SDS molecules, $\Sigma_{CH} b = -1.38 \times 10^{-12}$ cm. With $V_{CH} = 0.346 \text{ nm}^3$ (35), we obtain $\Delta \rho_m = 14.52 \times 10^{-14}$ cm, and thus with the data shown in Fig. 3, the hydrocarbon core mass per length:

$$M_{CH}/L = 5.89 \times 10^{-14} \text{ g/cm},$$

corresponding to 20.9 SDS molecules per nm, or a radius of 1.52 nm.

The latter value is appreciably smaller than the value of 1.9 nm estimated above. The discrepancy may have several alternative causes, for example, the headgroups of the surfactant micelles may give some contrast, which would mean that 1.9 nm is larger than the hydrophobic core radius. This

is corroborated by the fact that a radius of 1.54 nm can be calculated from the results in Ref. (17), Fig. 10, from SANS studies of perdeuterated SDS in water. If the latter value corresponds to the radius of the hydrophobic core of the micelle, a somewhat larger value would be expected from measurements of normal SDS in D_2O . On the other hand, the data in Fig. 3 would tend to overestimate the mass per unit length, and thence the radius, since the true contour length of the micelles would be longer than the estimates from the scattering curves. The reason for the deviations can possibly be a deviation from a circular cross-section of the cylinder or that the interface between the core and the aqueous environment is not sharp. The rod lengths are also expected to be highly polydisperse, and the different measurements of length are not weighted in the same way.

As a side comment, we note here that measurements of time-averaged light scattering intensities show a weak peak as a function of scattering vector, although the variations in the data are close to the experimental error in the points. The effect was sufficient to inhibit calculations of the radii of gyration and so we did not further pursue the analysis of the time-averaged intensities, but restrict the discussion below to the dynamic light scattering data. The location of the weak maximum appears, however, to be dependent on concentration and temperature and may thus reflect partial alignment of the rod-like micelles in solution, since it cannot have an electrostatic origin in 0.8 M salt. The position of the maximum on the q axis will then be related to the average distance between micelles and on the length scale of the interactions.

The dynamic scattering data for SDS at 25°C were first analyzed using inverse Laplace transformation (ILT) employing the algorithm REPES. Measurements were made at four concentrations at 16 angles. In all cases the relaxation time distributions were bimodal as shown by typical data in Fig. 4a for $C_{SDS} = 30 \text{ mM}$ in 0.8 M NaCl at angle 90°.

In the absence of complementary information regarding the conformation of the SDS micelle at 25°C (in particular our inability to determine the radius of gyration and molar mass from the time-averaged intensities), we follow the indications from the SANS data that a rod-like model may be applicable, and analyze the DLS data along these lines. While we do not infer that this is the correct model, it does represent a limiting case which is amenable to analysis. With the rigid-rod model, the slow mode should correspond to translational diffusion of the SDS micelle while the fast mode should correspond to the rotational dynamics of the micelle. The latter mode contributes about 15% of the total intensity at angle 90°, it has a nonzero intercept and its relative amplitude increases nonlinearly with q in accordance with the theoretical expectations for this model (36).

Typical behavior for the fast and slow modes is shown in Fig. 4b for four concentrations. It was found that the most consistent analysis pattern could be obtained by fitting the

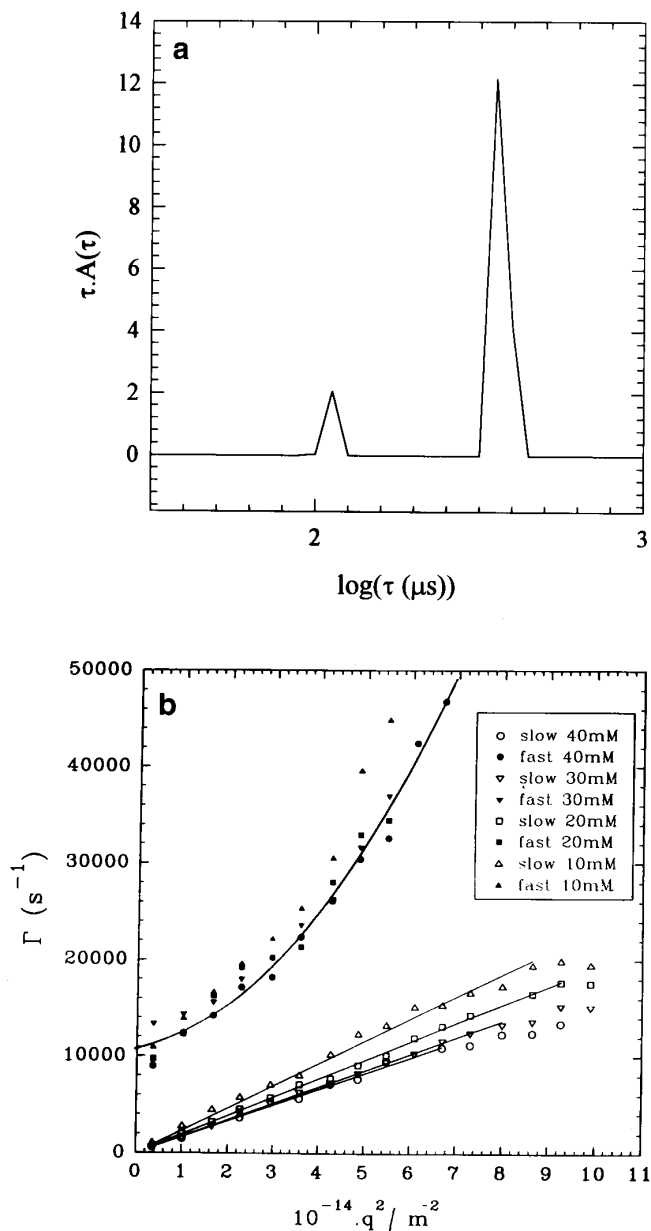


FIG. 4. (a) Relaxation time distribution through inverse Laplace transformation (REPES) of DLS data at angle 90° for an SDS solution $C = 30$ mM in 0.8 M NaCl at 25°C . (b) Results from a double-exponential fit to the $g_1(t)$ functions for SDS at the four concentrations shown. Open points are the slow translational diffusion, and filled points correspond to the fast rotational dynamics.

field correlation function ($g_1(t)$) to a double-exponential function. This was achieved by initially plotting as Γ_s versus q^2 —i.e. the relaxation rate of the dominant and well-defined slow exponential decay (Γ_s)—as a straight line passing through the origin. Then, using the autocorrelation function measured at each value of q , the corresponding Γ_s value was next employed as a fixed parameter in a double-exponential fit to extract the fast mode relaxation rate (Γ_f). This

is a substantially more precise method with many fewer degrees of freedom than inverse Laplace transformation using REPES and is particularly suitable here since it is known that there are only two contributing modes of relaxation. The data points shown for the fast relaxation in Fig. 4b were obtained in this way. To obtain the rotational diffusion coefficient, Θ , we have plotted, following Ref. (36), the apparent diffusion coefficient $D' (= \Gamma_f/q^2)$ versus $(1/q^2)$, which yields linear plots of slope 6Θ as illustrated in Fig. 5a. Figure 5b shows Θ versus SDS concentration.

Finally, we can make an estimate of the contour length using the expressions of Broersma for a rigid rod, length L and diameter $2R$, and in this way can compare the results with those from the SANS measurements fitted to a similar model, although the assumption of the rod model has obvious weaknesses in ignoring inherent flexibility and polydispersity effects. For more detailed discussions of analysis with application of the Broersma equations to DLS data, see Refs. (36, 37).

Using the approximate value of $R = 2$ nm for the micellar

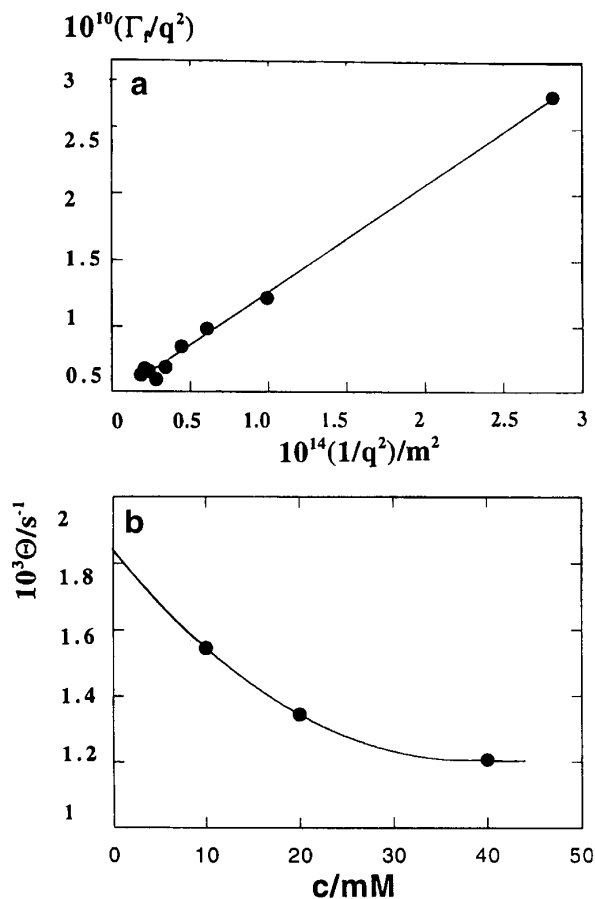


FIG. 5. (a) The apparent diffusion coefficient ($D' = \Gamma_f/q^2$) versus $(1/q^2)$ for the fast mode data at $C = 10$ mM in 0.8 M NaCl and at 25°C . The slope is 6Θ .³⁶ (b) The rotational diffusion coefficient (Θ) as a function of SDS concentration in 0.8 M NaCl and 25°C .

radius, together with the rotational diffusion coefficient, we obtain $L = 208$ nm at $C_{\text{SDS}} = 10$ mM, increasing to 226 nm at $C = 40$ mM in 0.8 M NaCl and at 25°C. At infinite dilution, $L = 197$ nm. From the Broersma equations for the translational diffusion coefficient, on the other hand, we obtain $L = 63$ nm at $C = 10$ mM increasing to $L = 88$ nm at $C = 40$ mM, which are significantly lower values. The discrepancy between the values of L from the two sources shows that the translational and rotational motions are coupled and are no longer independent. A significant diffusional anisotropy ($\Delta D = D_{\parallel} - D_{\perp}$) is detected. For 10 mM SDS, $D_{\parallel} = 2.82 \times 10^{-11}$ and $D_{\perp} = 2.05 \times 10^{-11}$ m² s⁻¹.

We note that the values of the contour length from the rotational diffusion coefficient are of the same magnitude as that deduced from the SANS data ($L = 160$ nm for $C_{\text{SDS}} = 30$ mM in 0.8 M NaCl at 25°C). The variations are attributed mainly to the low intensity of the rotational contribution in the DLS experiment, but the overall agreement in magnitude is gratifying.

Figure 6 shows representative decay curves from TRFQ measurements with 10 mM SDS in 0.8 μ M NaCl, at 45 and 25°C, respectively. The decay data are presented as (the logarithm of) $F(t)\exp(k_q t)$, i.e. in a form that corrects for the natural decay of the probe. In this representation, a constant level would be reached at long times, if the probes and quenchers were entirely confined to small micelles. With only long micelles, a continuous curvature should result. At the higher temperature the decay curve seems to approach, but not attain, a constant level, indicating that both shorter and longer micelles are present. The apparent aggregation number obtained by assuming the constant level to be given by the end of the recorded decay was about $N_{\text{aggr}} \approx 350$ at the lowest quencher concentration (0.028 mM), and decreased to 250 at the highest (0.047 mM; SDS concentration, 10 mM). Such a variation of the apparent aggregation number is to be expected in strongly polydisperse samples (38, 39).

From the aggregation number at 10 mM and 45°C, $N_{\text{aggr}} \approx 350$, we may calculate the length of the micelles, if we assume them to be cylinders with half-spherical endcaps. Taking the hydrophobic radius to be $R = 1.5$ nm the length is $L = 18$ nm; with a radius of 1.9 nm the length is 12 nm. The length deduced from the SANS measurements was 15 nm at the same concentration and temperature.

The decay curve at the low temperature shows the expected form for quenching in long rod-like micelles. The decay could be well fitted to the expression for one-dimensional quenching, which was not the case for the decay at 45 and 35°C (data not shown). The value obtained for the sum of the diffusion coefficients of the probe and quencher was $D = 4.3 \times 10^{10}$ m² s⁻¹, assuming the rod radius to be 1.5 nm as indicated by the SANS measurements. Since the D value depends critically on the value assumed for the radius, it should not be given too much significance. It is

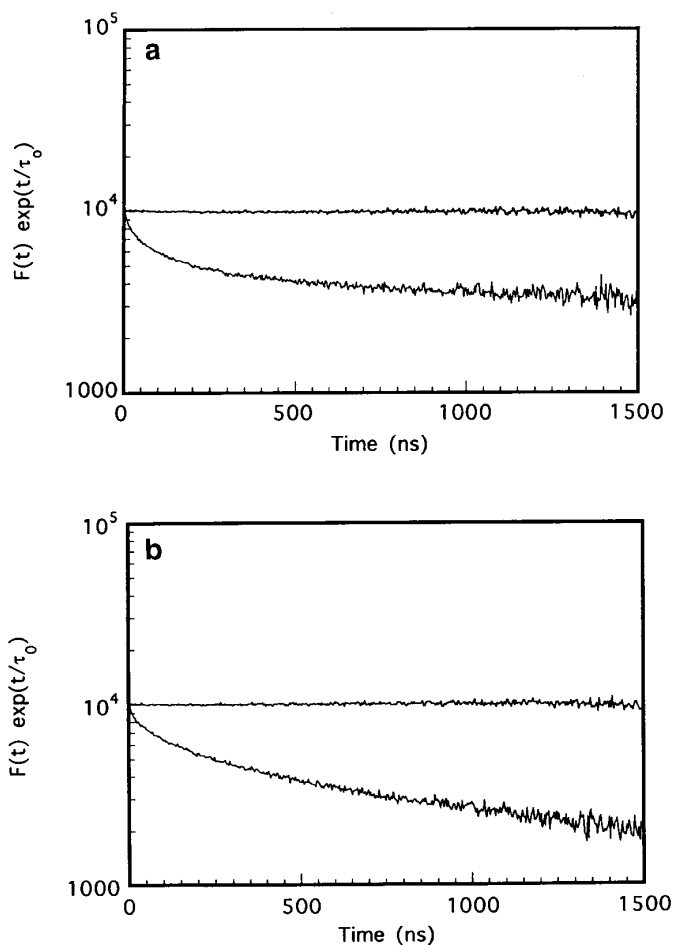


FIG. 6. Pyrene fluorescence decay curves, corrected for the natural decay of the probe to show the deactivation from quenching only. (a) At 40°C: 10 mM SDS, 0.8 M NaCl, 0.037 mM quencher, dimethylbenzophenone. (b) The same system at 25°C. In both figures the uppermost curve is the intensity of pyrene without quencher.

about a factor of 3 larger than that obtained previously for the same probe–quencher pair in rod-like micelles of the nonionic surfactant, C₁₂EO_x ($x = 5, 6, 8$); with a radius of 1.9 nm the values would agree. According to previous tests, decay curves from structures that in reality have large extensions in two dimensions give good fits to the one-dimensional model, but the resulting value for the diffusion coefficient is then unphysically large, by a factor of 10–100 (33).

The fluorescence quenching results are in good agreement with a growth from globular to cylindrical micelles when the temperature is decreased from 45 to 25°C and give no indication of growth in the width of the micelles. The size estimated for the micelles at the highest temperature agrees reasonably well with the SANS results.

Cryo-TEM. Four micrographs from the cryo-TEM study are presented in Fig. 7. No significant difference between D₂O and H₂O as the solvent was noted, and neither was any systematic difference observed depending on the tempera-

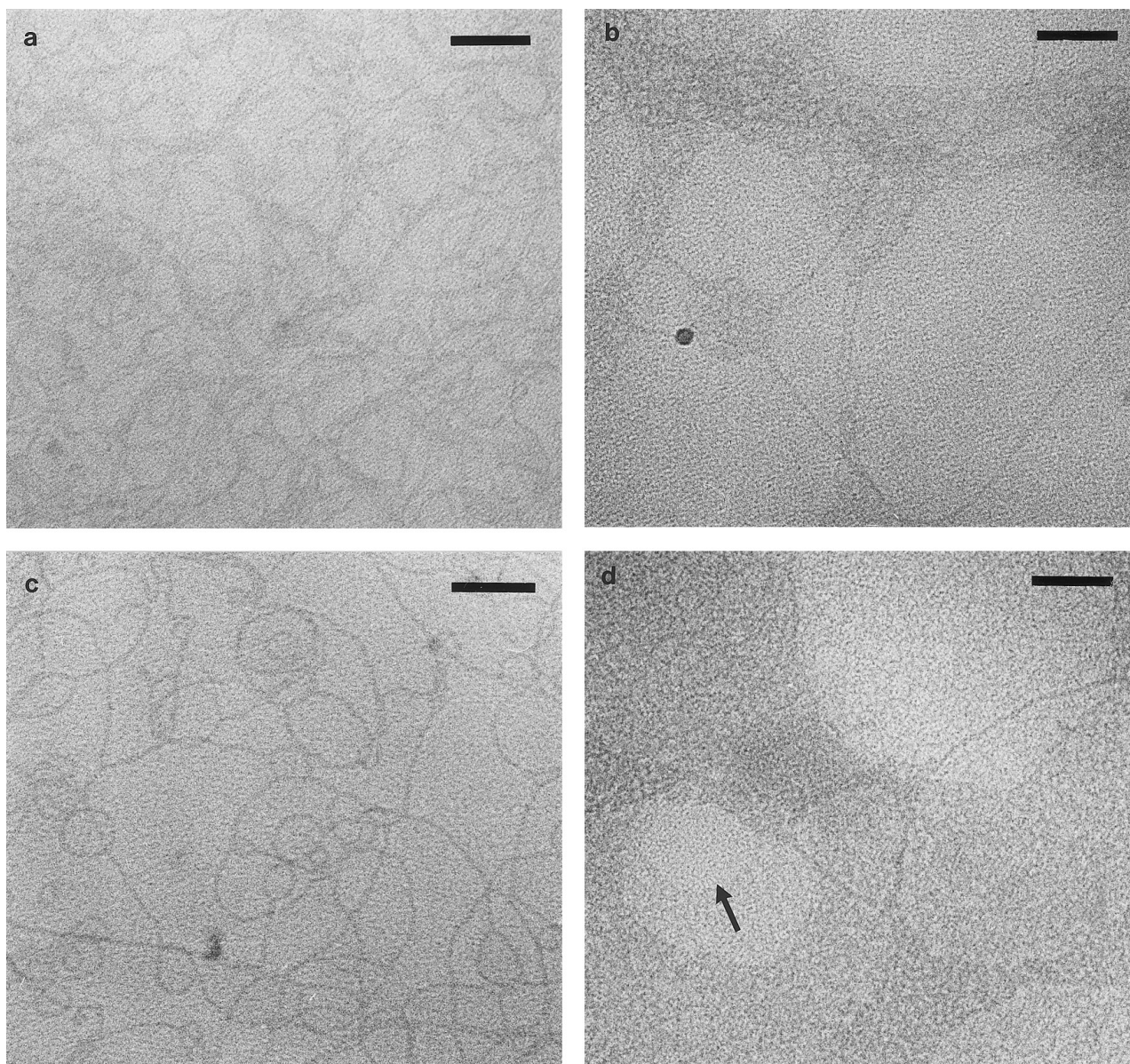


FIG. 7. Cryotransmission electron microscopy micrographs from several 30 mM SDS samples in 0.8 M NaCl. The four examples shown are vitrified from different temperatures between 55 and 25°C. No clear temperature dependence of the appearance of the structures could be seen, and no difference between water and D₂O as the solvent. We propose that these micrographs show interfacial structures, one set on each of the two air–water interfaces, and a background of smaller micelles from the bulk of the film. The arrow points on a patch without interfacial structures, dotted by small micelles; larger areas of this type are seen in b. Note that most of the long structures are much broader than 5 nm, which would correspond to a cylindrical micelle. The bar length corresponds to 100 nm.

ture from which the sample was vitrified. In b, which depicts a sample vitrified from 45°C, there is a dense background of small dots, representative of globular micelles. However, the micrograph also shows areas of highly entangled, almost lace-like, structures, connected by an open network of rather straight threads. On closer inspection, it appears as if two overlapping networks are present, suggesting that they may represent structures at the two air–water interfaces of the thin film. Also the micrograph from 25°C, d, seems to indi-

cate the presence of two overlapping two-dimensional structures. The lace-like patches are larger, but otherwise the sample structure is similar to that observed in b, and contrary to the expectations, areas showing small micelles (marked with arrow in Fig. 7c) are also observed at this low temperature. Occasionally, a loose network of entangled and looped threads, as exemplified in Fig. 7c, was observed during the cryo-TEM investigation. These structures may well represent long, flexible, cylindrical micelles, but the fact that no free

ends can be found, and that no sections show high contrast as would be seen for portions of the thread that extend perpendicular to the interface (such black patches are usually observed in samples of long cylinder structures (3)), together with the overall two-dimensional character of the image, suggest that adsorption at the air–water interface is responsible for the development of the aggregates.

In a careful study using NMR relaxation, self-diffusion measurements and, in addition, TRFQ (40), evidence for short rod-like micelles (axial ratio 6:1) were obtained for 2% SDS in 0.6 M NaCl at 25°C. Under the same conditions, Stüss *et al.* (41) made a cryo-TEM study, and concluded that long thread-like micelles were present. On closer inspection, however, the published micrograph is very similar (as far as the quality of print allows a comparison) to some of the micrographs obtained in our study, as exemplified in Fig. 7a. The long structures are clearly much broader than normal thread-like micelles and, moreover, seem to be confined to two dimensions, just as in our micrographs, again suggesting that we are dealing with a type of interfacial aggregate.

In any case, neither isolated, extended thread-like micelles, nor broad and interwoven secondary aggregates of such threads are consistent with the scattering and fluorescence data. Obviously, the peculiar structures from the cryo-TEM are not present in the fluid solutions, and must represent aggregates that appear either in the thin films, i.e. due to some interfacial effect, or due to a secondary aggregation process during the rapid cooling and vitrification. Moreover, the background of Fig. 7c, from low temperature, still appears dotted with small micelles, which could indicate that the concentration of surfactant in the interior of the film has decreased, due to adsorption at the interface.

In summary; in this system, the sample preparation method used in the cryo-TEM investigation does alter the dominant aggregate structure observed. The reason for this is not completely clear, but it appears as if the large surface area of the thin film, leads to a substantial adsorption at the air–water interface which depletes the bulk solution of surfactant, and causes the formation of extended, two-dimensional structures at the interfaces. However, the morphology of the aggregates at the air–water interface, and the driving force behind the adsorption, still remain to be thoroughly investigated.

CONCLUSION

The neutron scattering data demonstrate a rod-like local structure of SDS micelles at 25°C and also their limited length. Dynamic light scattering measurements have been also interpreted using the rod model, in which the fast decay reflects rotational contributions to the relaxation of the electric field correlation function $g_1(t)$. The TRFQ results confirm that high ionic strength, high surfactant concentration, and low temperature promote a sphere-to-rod transition of

SDS micelles. The unusual structures observed in the cryo-TEM examination are proposed to be present only at the interface of the thin samples, the formation possibly promoted by the cooling to low temperatures.

ACKNOWLEDGMENT

This work was supported by the Swedish Technical Research Council (TFR), in particular through a postdoctoral funding for J. C. Gimel.

REFERENCES

1. Reiss-Husson, F., and Luzzati, V., *J. Phys. Chem.* **68**, 3504 (1964); *J. Colloid Interface Sci.* **21**, 534 (1966).
2. Talmon, Y., *Ber. Bunsenges. Phys. Chem.* **100**, 364–372 (1996).
3. Almgren, M., Edwards, K., and Gustafsson, J., *Curr. Opinion Colloid Interface Sci.* **1**, 270 (1996).
4. Cabane, B., in "Surfactant Solutions. New Methods of Investigation" (R. Zana, Ed.), pp. 57, Surfactant Science Ser. 22. Marcel Dekker, New York, 1987.
5. Candau, S. J., in "Surfactant Solutions. New Methods of Investigation" (R. Zana, Ed.) pp. 147, Surfactant Science Ser. 22. Marcel Dekker, New York, 1987.
6. Magid, L., in "Dynamic Light Scattering" (W. Brown, Ed.), pp. 554. Clarendon Press, Oxford, 1993.
7. Schurtenberger, P., in "Light Scattering. Principles and Developments" (W. Brown, Ed.), pp. 293. Clarendon Press, Oxford, 1996.
8. (a) Mazer, N. A., Benedek, G. B., and Carey, M. C., *J. Phys. Chem.* **80**, 1075 (1976). (b) in "Micellization, solubilization, and microemulsions" (K.-L. Mittal, Ed.), Vol. 1, p. 359. Plenum Press, New York, 1977.
9. Missel, P. J., Mazer, N. A., Benedek, G. B., and Carey, M. C., *J. Phys. Chem.* **87**, 1264 (1983).
10. Young, C. Y., Missel, P. J., Mazer, N. A., Benedek, G. B., and Carey, M. C., *J. Phys. Chem.* **82**, 1375 (1978).
11. Murkerjee, P., *J. Phys. Chem.* **76**, 565 (1972).
12. Israelachvili, J., Mitchell, D. J., and Ninham, B. W., *J. Chem. Soc., Faraday Trans.* **72**, 1525 (1976).
13. Corti, M., and Degiorgio, V., *J. Phys. Chem.* **85**, 711 (1981).
14. Mishic, J. R., and Fisch, M. R., *J. Chem. Phys.* **92**, 3222 (1990).
15. Hayashi, S., and Ikeda, S., *J. Phys. Chem.* **84**, 744 (1980).
16. Ikeda, S., Hayashi, S., and Imae, T., *J. Phys. Chem.* **85**, 106 (1981).
17. Cabane, B., Duplessix, R., and Zemb, T., in "Surfactants in Solution" (K. L. Mittal and B. Lindman, Eds.), Vol. 1, p. 373. Plenum Press, New York, 1984.
18. Almgren, M., Alsins, J., Mukhtar, E., and Van Stam, J., *J. Phys. Chem.* **92**, 4479 (1988).
19. Almgren, M., *Adv. Colloid Interface Sci.* **41**, 9 (1992).
20. Moroi, Y., "Micelles: Theoretical and Applied Aspects." Plenum Press, New York, 1992.
21. Berne, B. J., and Pecora, R., "Dynamic Light Scattering." Wiley, New York, 1976.
22. Jakes, J., *J. Czech. J. Phys.* **B38**, 1305 (1988).
23. Nicolai, T., Brown, W., Johnsen, R. M., and Stepánek, P., *Macromolecules* **23**, 1165 (1990).
24. Johnsen, R. M., in "Laser Light Scattering in Biochemistry" (S. E. Harding, D. B. Sattelle, and V. A. Bloomfield, Eds.). The Royal Society Chemistry, Cambridge, 1992.
25. Provencher, S. W., *Makromol. Chem.* **180**, 201 (1979).
26. Jacrot, E., and Zaccai, G., *Biopolymers* **20**, 2413 (1981).
27. Benededouch, D., Chen, S.-H., and Koehler, W. C., *J. Phys. Chem.* **87**, 2621 (1983).

28. Sheu, E. Y., Wu, C.-F., and Chen, S.-H., *J. Phys. Chem.* **90**, 4179 (1986).
29. Guinier, A., and Fournait, G., "Small-Angle Scattering of X-rays." Wiley, New York, 1955.
30. Almgren, M., Hansson, P., Mukhtar, E., and van Stam, J., *Langmuir* **8**, 2405 (1992).
31. Infelta, P. P., Grätzel, M., and Thomas, J. K., *J. Phys. Chem.* **78**, 190–195 (1974).
32. Tachiya, M., *Chem. Phys. Lett.* **33**, 289 (1975).
33. Medhage, B., and Almgren, M., *J. Fluorescence* **2**, 7–21 (1992).
34. Vethamuthu, M. S., Almgren, M., Bergenståhl, B., and Mukhtar, E., *J. Colloid Interface Sci.* **178**, 538 (1996).
35. Tanford, C., "The hydrophobic effect," 2nd ed. Wiley, New York, 1982.
36. Claire, K., and Pecora, R., *J. Phys. Chem.* **101**, 746 (1997).
37. Schillén, K., Brown, W., and Johnsen, R. M., *Macromolecules* **27**, 4825 (1994).
38. Warr, G. G., and Grieser, F. G., *J. Chem. Soc., Faraday Trans. 1* **82**, 1825 (1986).
39. Almgren, M., and Löfroth, J.-E., *J. Chem. Phys.* **76**, 2734 (1982).
40. Söderman, O., Jonströmer, M., and van Stam, J., *J. Chem. Soc., Faraday Trans.* **89**, 1759 (1993).
41. Süss, D., Cohen, Y., and Talmon, Y., *Polymer* **36**, 1809 (1995).